Magnesium and magnesium alloy dissolution by high intensity focused ultrasound: erosion/cavitation vs. Wave propagation

Noura Sleiman, Rachel Pflieger, Loïc Hallez, Sergey I Nikitenko, Jean-Yves Hihn

Ultrasonics Sonochemistry 104 (2024) 106836

Contents lists available at ScienceDirect

Ultrasonics Sonochemistry

journal homepage: www.elsevier.com/locate/ultson

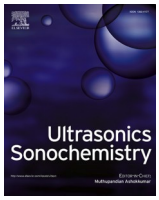

Magnesium and magnesium alloy dissolution by high intensity focused ultrasound: erosion/cavitation vs. Wave propagation

Noura Sleiman [a,b,c], Rachel Pflieger [b], Loïc Hallez [a], Sergey I. Nikitenko [b], Jean-Yves Hihn [a,c,*]

[a] Université de Franche-Comté, CNRS, Institut UTINAM UMR 6213, F-25000 Besançon, France
[b] ICSM UMR 5257 – CEA, Univ Montpellier, CNRS, ENSCM, Bagnols-sur-Cèze, France
[c] IRT M2P, Metz, France

ARTICLE INFO

Keywords:
Magnesium
Magnesium alloys
High-intensity focused ultrasound
Cavitation
Acoustic streaming
Dissolution
Surface roughness
Microstructure analysis

ABSTRACT

The dissolution of metals, influenced by mechanical and chemical factors, plays a crucial role in various applications. Ultrasonic irradiation has been explored for its ability to enhance dissolution rates and modify surface characteristics. In this study, we investigate the dissolution of magnesium (Mg) and magnesium alloys under high-intensity focused ultrasound (HIFU) conditions with frequency sweeping (wobbling). Our findings reveal distinct effects of cavitation and acoustic streaming on the dissolution process. For pure magnesium, ultrasonic treatment significantly increases dissolution rates compared to silent conditions. Negative frequency sweeps result in the highest dissolution rates, linked to increased cavitation activity, while positive sweeps reduce dissolution rates but maintain acoustic streaming effects. The removal of surface oxides is accelerated in all sonication conditions. Macro- and micro-roughness patterns on the surface correspond to the wobbling frequency range, with wavelengths matching the average ultrasonic frequency. However, dissolution is not uniform across the sample, and preferential attack occurs at the focal point during negative frequency sweeps. In contrast, magnesium alloys exhibit lower dissolution rates than pure Mg. The alloy's mechanical properties make it less susceptible to cavitation erosion but more sensitive to acoustic streaming-induced dissolution. Grain boundaries are preferentially attacked, revealing differences between ductile pure Mg and the harder, more cavitation-resistant, alloy. This study highlights the complex interplay between cavitation and acoustic streaming in the dissolution of magnesium and its alloys under HIFU conditions, shedding light on the limits and potential applications of this technique, particularly in microstructure analysis.

1. Introduction

Dissolution of metals is a phenomenon sensitive to many parameters: mechanical and chemical effects and their combination. The mechanical effects are directly related to the increase in material transfer at the interface, as seen in previous works on zinc dissolution where ultrasound is particularly effective such as zinc enhanced corrosion [1] or particles dissolution [2]. This process is sought in many cases for dissolution acceleration [3–5], and ultrasound plays a key role when the impact of mass transfer is of primarily importance [6]. If this concerns mostly the electrolyte layer close to the surface, it can be extended in some specific cases to the liquid trapped into porosities close to the substrate surface, inducing the so-called ultrasonic-capillarity effect [7]. The transition to solution is not the only expected effect. Control of ultrasonic parameters is of primary importance for control of crystallization or fragmentation, as well as in the case of solid particle nucleation and growth [8], where expectations go well beyond mean dissolution rates.

These changes in surface state have been reported [9] to accompany changes in morphology. Coupling with chemical compounds has also been implemented, as in the case of dissolution of oxides in acidic media [10]. Sonication can be used in the case of accelerated corrosion tests [11,12], with promising cases of dissolution under tension [1]. In a few hours it is possible to mimic the corrosion facies usually obtained after weeks of natural exposure. Ultrasonic irradiation can also be used to mimic exposure to hydrodynamic cavitation (propellers, pumps, etc.) with studies on the effects of shock waves generated by bubbles collapsing close to the surface [13]. Work was taken to the point of surface texturing, with Mg as a model element. Ji et al. were able to control the surface to create "golf ball patterns", with perspectives in

* Corresponding author.
E-mail address: jean-yves.hihn@univ-fcomte.fr (J.-Y. Hihn).

https://doi.org/10.1016/j.ultsonch.2024.106836
Received 26 October 2023; Received in revised form 7 February 2024; Accepted 27 February 2024
Available online 28 February 2024

tribology and protection [14]. Magnesium and its alloys present a particular relevance, with gentle dissolution in low-aggressive acids.

While control of the surface by ultrasonic irradiation has been acknowledged as promising, to reach a higher fineness an increase in US frequency is required. Indeed, increasing frequency decreases wavelength allowing higher spatial resolution. Only very few works were carried out at very high frequencies due to the low acoustic energies available. High-intensity focused ultrasound (HIFU) overcomes this limitation by concentrating acoustic energy at the focal point, making it possible to go beyond the cavitation threshold for a wide range of high frequencies (1 MHz to 4 MHz). This has been largely described in the literature [15–19]. In HIFU geometry, distribution of acoustic energy and cavitation is specific, as bubbles present in the focal zone shift the activity towards the transducer [20,21]. Additionally, control of the excitation signal is possible, making it possible to either enhance or quench the cavitation activity by sweeping frequency (wobbling [19,22]).

Recent works have investigated mechanisms of cavitation activity enhancement under frequency sweep. The method consists of exciting the transducer at a fixed frequency called F_{start}, most often chosen in the transducer bandwidth, then varying it to a higher (positive frequency sweep $\Delta F > 0$) or smaller frequency (negative frequency sweep $\Delta F < 0$). The rate of the frequency change is a determining parameter, as well as the final frequency of the sequence, called F_{stop}. The return to the F_{start} frequency is done quite instantaneously (no sweep mode in this direction). Effects on sonoluminescence (and therefore on cavitation activity) are impressive, as describe in previous works [23,24]. While sonochemiluminescence (SCL) measurements, as well as cavitation noise spectra, confirm the variation in cavitation activity i.e. presenting the same attenuation (under positive scan) or intensification (under negative scan), a more thorough investigation of sonoluminescence (SL) spectra does not show any particular behavior [25]. Even if it was the first time that molecular emissions were reported at such high frequency, the resulting characteristics of the plasma do not show any spectral difference when wobbling is applied. Thus, it was concluded that changes in cavitation activity were linked to the number of active bubbles and to the activation of more bubble nuclei [23–25].

Therefore, in the global objective of understanding the respective effects of erosion due to bubble collapse and shock waves and the dissolution due to wave displacement and acoustic streaming at the surface, the present work intends to reproduce these conditions of exposure with HIFU modulated by sweeping frequency. It will therefore be possible, with HIFU in wobbling mode, to compare the effects at the focal (where cavitation, erosion, micro-jets and shock waves take place) and on the rest of the sample (where agitation related to the movements of the boundary layer with the propagation of the waves occurs). Use of magnesium will be an opportunity to observe these interactions, especially in the case of wobbling, due to its ability to dissolve when exposed to both phenomena. Finally, a magnesium alloy will be studied to investigate the particular case of preferential etching in grain boundaries [26].

2. Experimental details

The irradiation process was carried out in a cubic plexiglass reactor in which a High-Intensity-Focused-Ultrasound (HIFU) designed by IMASONIC (Besançon, France) was set in the horizontal side. The HIFU was powered by an Agilent 33220A multi-frequency generator and an AR Worldwide® 150A100B signal amplifier of 150 W. Using a 3-axis support (x, y, z), the sample was fixed perpendicularly to the acoustic axis of the HIFU with a distance of 4 cm so that the focal zone was in the center of the sample surface. The magnesium disc was then inclined by an angle of 45° to avoid reflections. An oscilloscope (Lecroy WaveSurfer 44Xs, 400 MHz, 2.5 GS/s) was used to ensure correct positioning of the sample by echolocation (Δt 54 μs) (Fig. 1).

Magnesium discs (99.97 % purity) and AZ31 magnesium alloy discs (96 % magnesium, 3 % aluminum, 1 % zinc) were purchased from Goodfellow. Before sonication, each sample was cut to a diameter of 9 mm and a thickness of 1.5 mm and mechanically polished with diamond suspension up to 1 μm in order to attain mirror surface (arithmetical average of profile height deviations from the mean line $R_a = 0.179$ μm), before being cleaned with ethanol and deionized water and dried out. In order to ensure that all observations correspond to the same orientation, a marker was made by indentation (SOMECO) on each surface prior to all experiments, and samples were reproducibly placed in the set-up with the marker at the top.

The aqueous solutions were prepared with deionized water (Milli-Q 18.2 MΩ cm). For all experiments, metal discs (pure magnesium or alloy) were submerged in 5 L of 0.1 M oxalic acid (Alfa Aesar) at room temperature and atmospheric pressure for a total duration of 20 min with continuous sparge of air, allowing saturation and therefore controlled experimental conditions. Sonication was stopped at regular

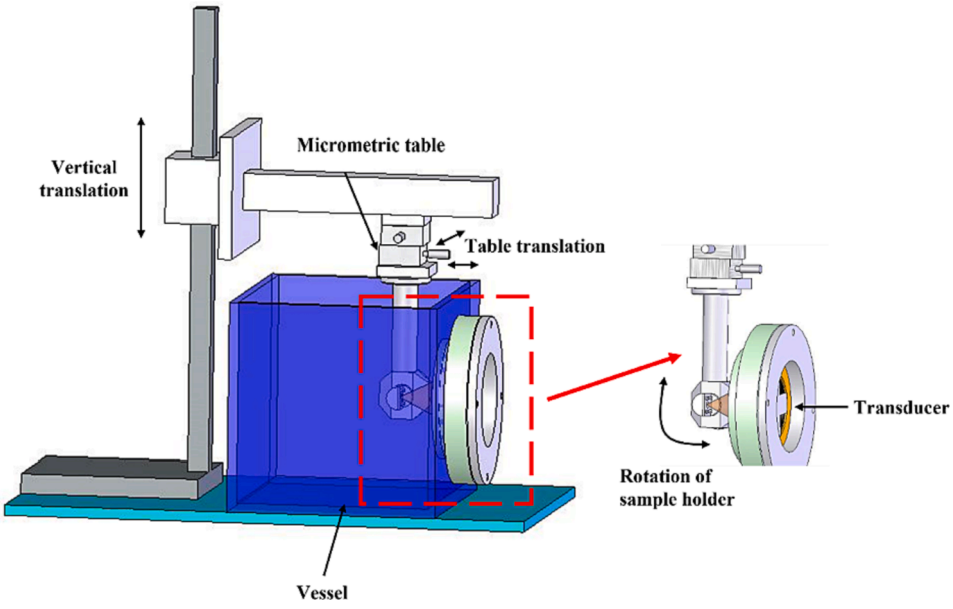

Fig. 1. Schematic of the experimental set-up [19].

intervals to monitor the evolution of samples with a systematic set of characterizations (mass loss, visual observation, optical microscopy, interferometry). The mass was measured before and after every irradiation using a digital balance with 10^{-4} g precision. Pictures of the surfaces were taken with a camera and with a digital optical microscope (HIROX). Additional characterizations were made with SEM/EDS (Scanning Electron Microscopy - Energy Dispersive X-ray Spectroscopy, Tescan MIRA 3), AFM (Atomic Force Microscopy, Nano-Observer CSI) and profilometry (Profilm 3D). The average height difference between neighboring peaks and valleys (Rc) was extracted from the profiles. Analysis of the dissolved magnesium was conducted by ICP (Inductively Coupled Plasma, ICP-OES VARIAN 720 ES - Axial) to obtain surface dissolution rates.

Three different irradiation conditions were studied and compared to silent conditions (without ultrasound) for both pure and alloyed magnesium: at a fixed frequency of 3.6 MHz ($\Delta F = 0$), under negative frequency sweep, and under positive frequency sweep. For both sweeping conditions, 3.6 MHz was used as the start frequency. Under negative frequency sweep ($\Delta F < 0$) F_{stop} (frequency at the end of the sweep) was 3.44 MHz, sweep rate − 80 MHz/s and sweep time 2 ms. Under positive frequency sweep ($\Delta F > 0$) F_{stop} was 3.76 MHz, sweep rate + 80 MHz/s and sweep time 2 ms. For all these conditions, the transmitted power was always kept between 8.9 and 9.4 W [24].

3. Results and discussion

3.1. Pure magnesium

Magnesium is known to be easily oxidized in the presence of oxygen or an aqueous solution, whereby it forms an oxide or hydroxide surface layer (Eq. (1) and Eq. (2)) [27]:

$$Mg + 1/2\,O_2 \rightarrow MgO \quad (1)$$

$$Mg + 2H_2O \rightarrow Mg(OH)_2 + H_2 \quad (2)$$

This process can be accelerated in the presence of an acid that will shift reaction (2) or under ultrasonic irradiation resulting in dissolution of the formed oxidized layer [14,27]. Therefore; global dissolution is enhanced, which can be followed by mass loss or by Mg^{2+} concentration in the solution. Fig. 2 presents the mass loss in mg after 20 min of ultrasonic irradiation for four pure Mg discs under different irradiation conditions, and the corresponding calculated thickness decrease rates.

All data were confirmed by ICP measurements (not shown here).

In silent conditions, the mean dissolution rate in 0.1 M oxalic acid is about 3.1 μm/min corresponding to 14 μmol/min, in good agreement with the 11.3 μmol/min previously obtained in 0.001 M oxalic acid [11]. It is to be noted that, while these initial rates (in the first tens of minutes) show a low sensitivity to the oxalic acid concentration, an increase in treatment time may result in a higher impact of acid concentration due to H^+ consumption. In the presence of ultrasound, dissolution rates strongly increase, irrespective of the irradiation parameters. As expected from previous studies with sonoluminescence (SL) and sonochemiluminescence (SCL) as output parameters [23–25], the highest value (13.4 $\mu m.min^{-1}$) is obtained with a negative frequency sweep, and the lowest one with a positive sweep. An increase of about 30 % is noticed for the mean thickness loss rate under negative sweep compared to fixed frequency, while it decreases by about 13 % under positive sweep.

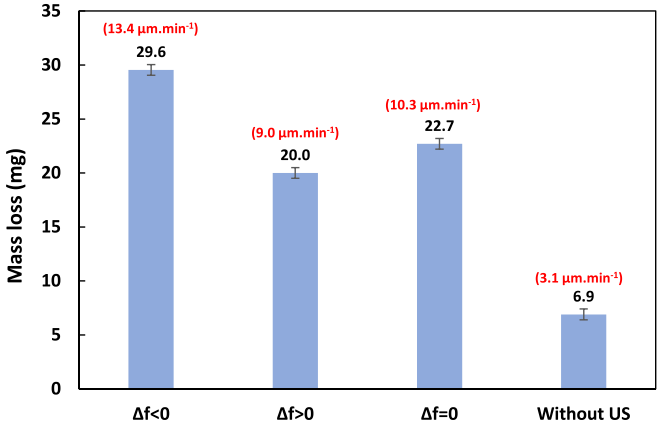

Fig. 2. Histogram of mass loss (mg) and dissolution rate (μm.min-1) of pure magnesium after 20 min of irradiation in 0.1 M oxalic acid under: $\Delta F < 0$ (3.6–3.44 MHz, 2 ms, −80 MHz/s sweep rate), $\Delta F > 0$ (3.6–3.76 MHz, 2 ms, +80 MHz/s sweep rate), $\Delta F = 0$ (3.6 MHz) and without ultrasound, with the corresponding thickness decrease rates noted between brackets.

In SL and SCL experiments, intensity, related to inertial cavitation, was extremely high under negative frequency sweep and quenched under positive sweep [23,24]. Sleiman et al [25] explained such enhancement and quenching in cavitation activity by changes in the number of cavitation bubbles, which were not related to any apparent change in the nature of the intra-bubble plasma. On the contrary, dissolution is not quenched with a positive sweep because HIFU combines cavitation activity and acoustic streaming [19]. The latter remains active in the $\Delta F > 0$ case.

The appearance of the discs submitted to the four different conditions is exemplified in Fig. 3. Except for the disc treated under silent conditions, all others present bright surfaces with a rippled texture. The presence of a hole at the center of the disc exposed to negative frequency sweep was already observed after 10 min sonication time. This corresponds to a local dissolution rate of about 150 $\mu m.min^{-1}$ and illustrates the strong heterogeneity of the erosion, which is particularly intense at the focal zone under $\Delta F < 0$.

SEM pictures of the same samples confirm these observations (Fig. 4). In the case of silent conditions, the surface is covered by grey oxides that are removed in all sonication conditions.

These oxides are removed even in the absence of cavitation ($\Delta F > 0$), which indicates that acoustic streaming combined with acidic conditions is sufficient to remove the oxide layer. SEM pictures allow better visualization of the ripple pattern (Fig. 4a,b,c), with a nice concentric ring organization in the case of the negative frequency sweep. It is important to bear in mind that all samples were positioned parallel to the transducer with a 45° angle to the vertical axis to avoid reflection towards the transducer. A consequence of this is a dissymmetry between the left and right sides of the impact, inducing discrepancies in the surface pattern, particularly visible when the convectional flow is large (Fig. 4 b&c). A zoom was carried out on two particular cases (Fig. 5). The first one under silent conditions confirms the presence of corrosion products irregularly distributed on the surface (Fig. 5a). EDS analyses indicate that white zones (Z1) are pure metal (>90 % Mg), whereas dark gray ones (Z2) correspond to oxides (around 50 % Mg). On the contrary, after sonication, the surface is free of oxides, and grain structures are clearly visible (Fig. 5b). It has to be noticed that, irrespective of exposure conditions, no preferential attack of grains or grain boundaries is visible.

During ultrasonic irradiation, micro-roughness decreases, as highlighted by the increasing brightness. On the other hand, a macro-roughness appears, evidenced by the ripple organization. Looking closer at the ripple organization on the right side of the $\Delta F < 0$ sample, a profilometry surface analysis (Fig. 6a & 6b) reveals a succession of regularly arranged peaks and valleys. The 2D and 3D surfometry pictures show large valleys around 100-μm-wide, separated by relatively sharp peaks. A profile was extracted along the radial axis (red line in Fig. 6a), from which several parameters were determined.

The resulting profile is plotted in Fig. 7 and allows determination of a surface oscillation wavelength (peak-to-peak) of 213 μm. The amplitude of the oscillations was quantified with a mean height of profile elements Rc of 37 μm.

These determinations were repeated for all ultrasonic conditions in the zones where ripples are well organized, and are summarized in

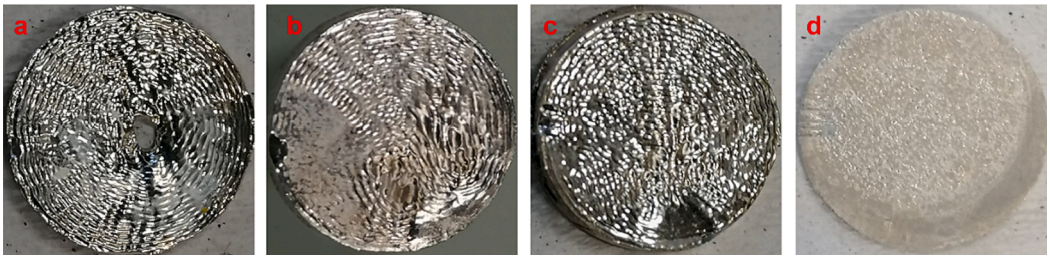

Fig. 3. Photographs of pure magnesium discs after 20 min of irradiation in 0.1 M oxalic acid under a) negative frequency sweep (3.6–3.44 MHz 2 ms), b) positive frequency sweep (3.6–3.76 MHz 2 ms), c) fixed frequency (3.6 MHz), d) silent conditions.

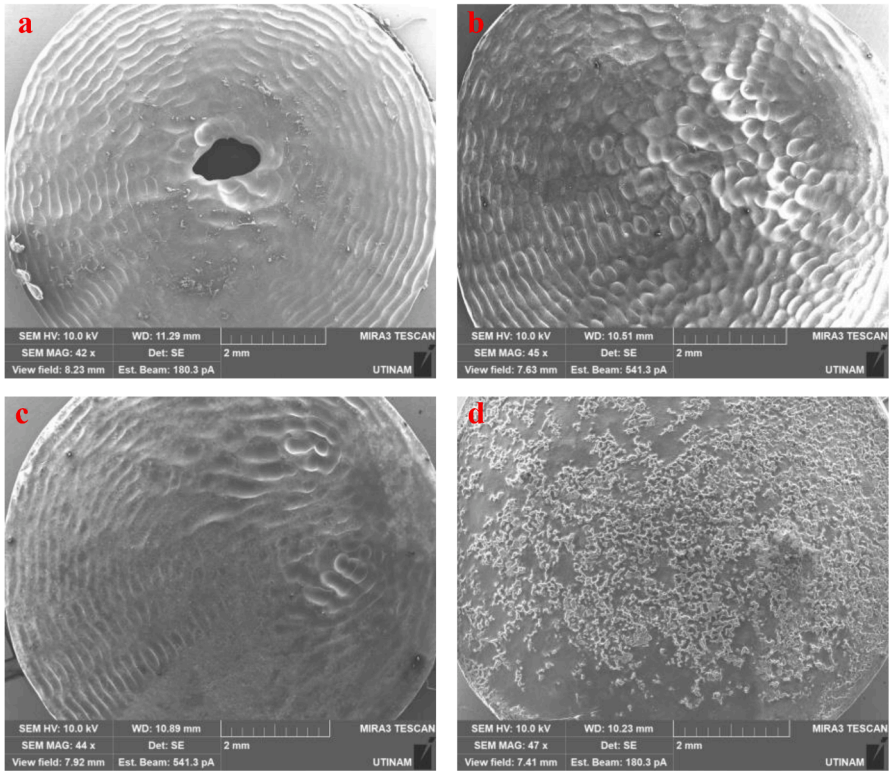

Fig. 4. SEM images of pre magnesium surfaces after 20 min of irradiation in 0.1 M oxalic acid under. a) $\Delta F < 0$ 3.6–3.44 MHz (2 ms). b) $\Delta F > 0$ 3.6–3.76 MHz (2 ms). c) $\Delta F = 0$. d) without US.

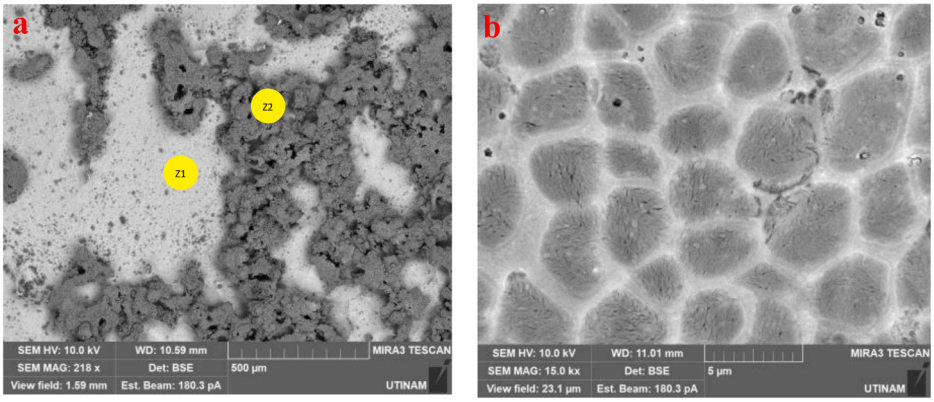

Fig. 5. SEM images of pure Mg surfaces after 20 min of irradiation in 0.1 M oxalic acid under a) silent conditions, b) $\Delta F > 0$ 3.6–3.76 MHz (2 ms).

Table 1. The experimentally determined surface oscillation wavelength is systematically compared to the half-wavelength corresponding to the mean frequency of the scanned interval. Interestingly, the peak-to-peak distance (surface oscillation wavelength) matches with the theoretical $\lambda/2$ derived from the average ultrasonic frequency, irrespective of the sweeping conditions. Wherever the ripple pattern is well organized,

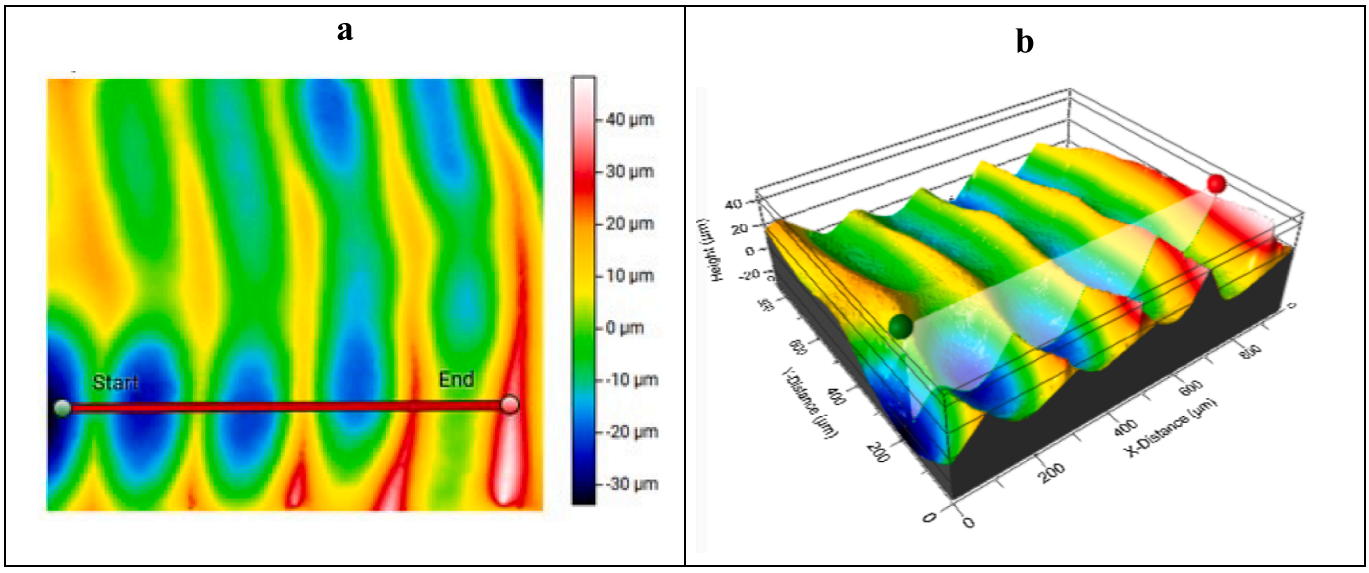

Fig. 6. Pure magnesium surface profile after 20 min of irradiation in 0.1 M oxalic acid under negative sweep 3.6–3.44 MHz (2 ms), measured with an interferometer: a) 2D profile, b) 3D profile.

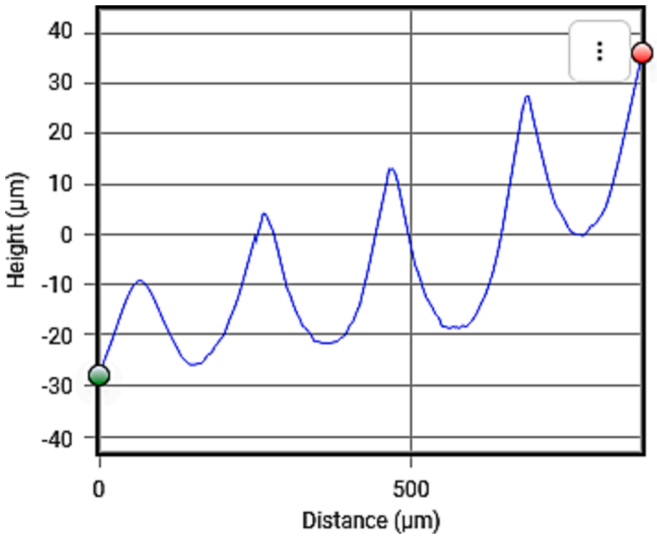

Fig. 7. Topographic profile of the magnesium surface depicted in Fig. 6 after 20 min of irradiation in 0.1 M oxalic acid under negative sweep 3.6–3.44 MHz (2 ms).

Table 1
Oscillation period and half acoustic wavelength for pure Mg under $\Delta F < 0$, $\Delta F > 0$ and $\Delta F = 0$.

Conditions	Irradiation conditions	Mean frequency, MHz	Theoretical $\lambda/2$, µm	Surface oscillation wavelength, µm	R_c, µm
$\Delta F < 0$	3.6–3.44 MHz 2 ms	3.52	213	213	37
$\Delta F > 0$	3.6–3.76 MHz 2 ms	3.68	204	204	35
$\Delta F = 0$	3.6 MHz	3.6	208	207	19

dissolution is controlled by the mean ultrasonic frequency. Nevertheless, the large differences observed in the dissolution rates result in a dependence of roughness on the sweeping mode. However, it should be borne in mind that this measurement is local and restricted to a particular well-organized zone, which cannot be extended to the whole sample surface. For instance, dissolution is not homogeneous, with a very high rate at the center for $\Delta F < 0$ and presence of undulations for $\Delta F > 0$ and $\Delta F = 0$.

Looking more precisely on a zone surrounding a peak (Fig. 8 at a fixed frequency of 3.6 MHz), a secondary ripple organization on a smaller scale appears on both sides of the peak. Moreover, a high degree of roughness is present on its top. In order to determine if these patterns are dependent on wavelength on a lower scale, which may result from subharmonics of the mean frequency, the same profilometry surface analysis as in Fig. 6 was conducted.

The 2D and 3D surfometry pictures (Fig. 9) confirm that peaks are very sharp, separating large basins with height differences exceeding 50 µm. Oscillations are also visible on the edges on the 3D profile (Fig. 9b), and a profile was extracted along the radial axis indicated by a red line in Fig. 9a to extract roughness parameters.

The profile along the red line is presented in Fig. 10a. A steep slope can be seen on the ripple part closest to the peak. A roughness is visible in the slope, but quite low compared to the size of the ripples described

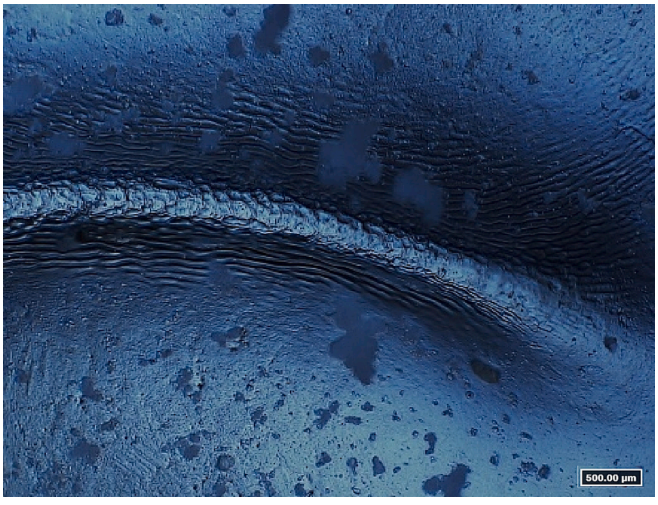

Fig. 8. Detail of a ripple on a pure magnesium surface after 20 min of irradiation in 0.1 M oxalic acid under fixed frequency of 3.6 MHz (numeric optical microscopy, x700).

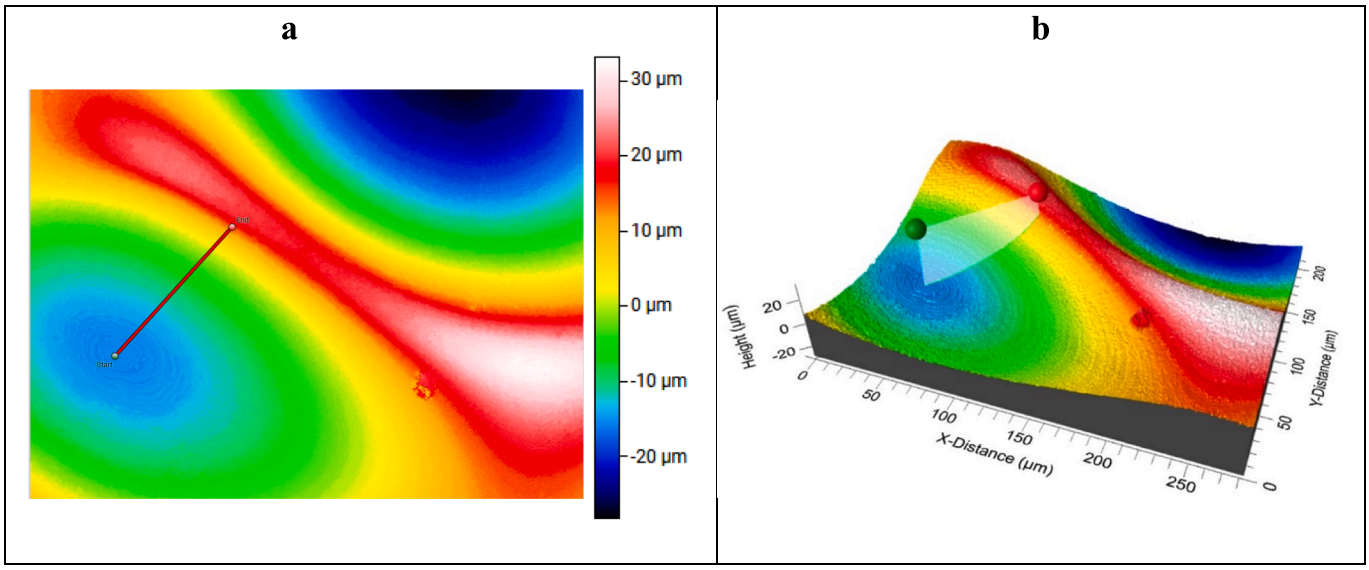

Fig. 9. Pure magnesium surface profile focused on a peak, after 20 min of irradiation in 0.1 M oxalic acid under positive sweeping 3.6–3.76 MHz (2 ms), measured with an interferometer: a) 2D profile, b) 3D profile.

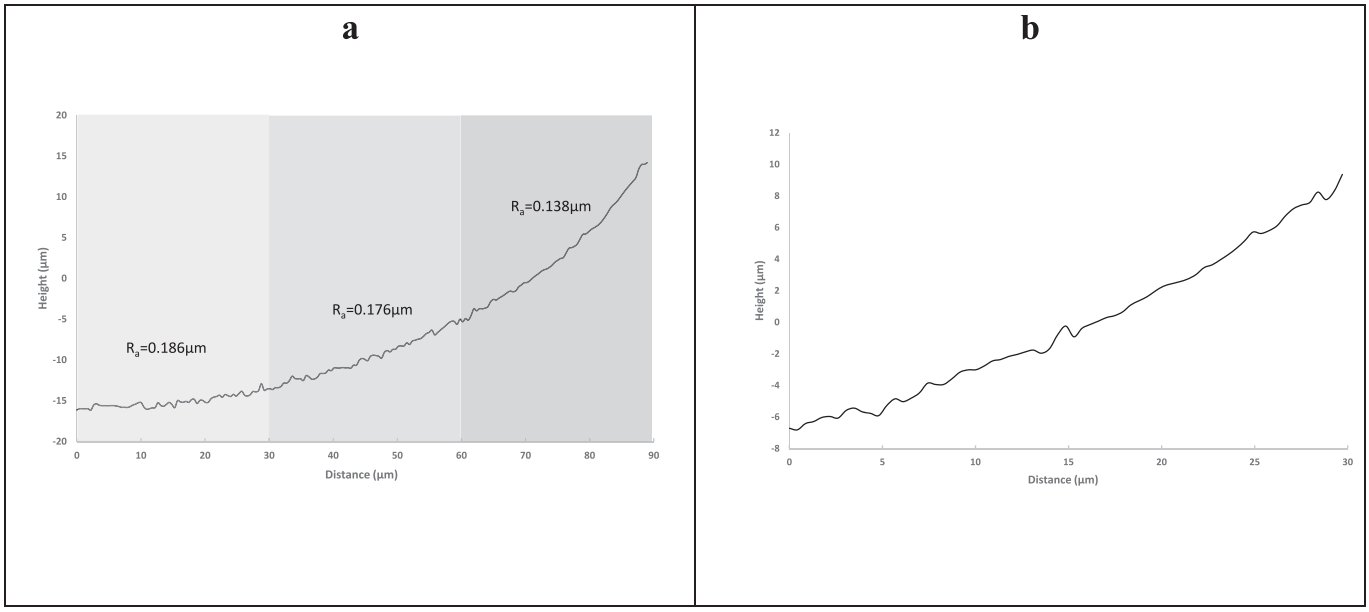

Fig. 10. Micro-roughness profile measured with an interferometer of a pure magnesium surface after 20 min of irradiation in 0.1 M oxalic acid under positive sweeping 3.6–3.76 MHz (2 ms). a) full profile (Fig. 9) with roughness measurement Ra for each profile segment b) zoom on the first segment starting from the left.

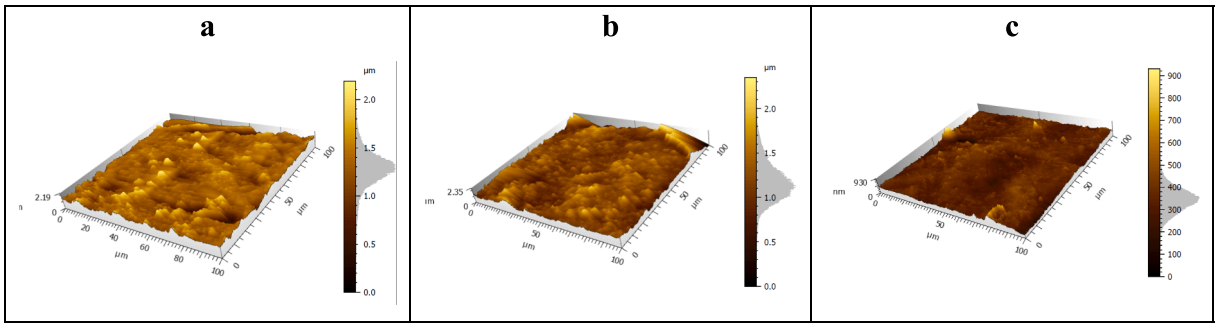

Fig. 11. AFM images for the surface of a pure magnesium surface after 20 min of irradiation in 0.1 M oxalic acid under a) ΔF < 0–3.6–3.44 MHz (2 ms) b) ΔF > 0–3.6–3.76 MHz (2 ms) c) ΔF = 0–3.6 MHz.

previously. Its value is calculated for 3 slope segments, equally distributed in Fig. 9a. One of these segments is shown in Fig. 10b, and it can be observed that the peaks are not organized according to the US wavelength or a multiple value; they would thus correspond to remains of the initial roughness, namely 0.179 μm.

To consider micro-roughness, AFM measurements were performed using an App NaNo tip with a size < 10 nm and a height of 14–16 μm (Fig. 11). Only peak tops were considered due to the impossibility to take measurements in the valleys. Images were taken at 100 × 100 μm in several zones for each sample, revealing no significant dependence on the frequency sweep mode. A high degree of roughness was observed with a peak height distribution centered between 1.5 and 1.0 μm (Fig. 11 a. and 11b.) and an arithmetical average of height deviations from the mean surface Sa, respectively of 0.125 μm for ΔF < 0 and 0.12 μm for ΔF > 0 (taken from 3 zones per condition).

More surprising are the results at a fixed frequency of 3.6 MHz, with peak height distribution centered between 0.5 and 0.25 μm (Fig. 11 c.) and a lower arithmetical average of height deviations from the mean surface Sa of about 0.07 μm (taken from 3 zones). Concerning AFM pictures, the absolute difference is very low, and we can conclude only on a slight chemical polishing effect on the peak tops (more exposed to the electrolyte) in comparison with the initial roughness values of Sa = 0.18 μm.

3.2. Magnesium alloy

In the same way as for pure Mg discs, Fig. 12 presents the mass loss after 20 min of ultrasound irradiation for Mg alloy discs under different irradiation conditions, as well as the corresponding calculated thickness decrease rates.

The first finding is that dissolution rates are significantly lower than for pure Mg. In silent conditions, the mean dissolution rate is three times lower, 0.9 μm.min-1 instead of 3.1 μm/min, indicating that the alloy is more acid-resistant. This higher resistance to dissolution is confirmed under ultrasound, although the difference is somehow less marked, by about twice, for constant frequency and both sweeping directions. Contrary to pure Mg, the Mg alloy is sensitive likewise to the increase in local cavitation activity (ΔF < 0) and to the increase in acoustic streaming and agitation by convection (ΔF > 0). Although the cavitation activity largely increases by ΔF < 0, as brought to light by previous sonoluminescence (SL) and sonochemiluminescence (SCL) measurements [25], it does not lead to an increased mass loss, indicating a change in the dissolution mechanism, the alloy appearing to be less sensitive to cavitation erosion. This can be explained by its mechanical properties, and in particular its hardness that is much greater than that of pure Mg (73 Hv vs. 30–35 Hv). Grain size variation, which is on the same range of magnitude in both case (around 4–5 μm), cannot be incriminated.

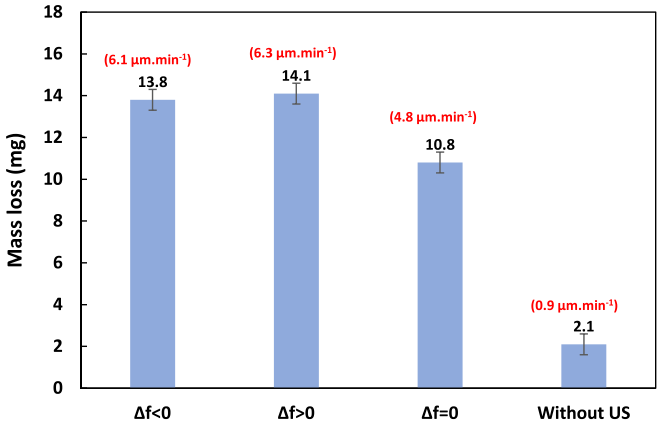

Fig. 12. Histogram of the mean dissolution rates (μm. min $^{-1}$) of magnesium alloy AZ31 after 20 min of irradiation in 0.1 M oxalic acid under different irradiation conditions ΔF > 0, ΔF < 0, ΔF = 0 and without ultrasound.

Fig. 13 shows pictures of the surface after exposure to the four different conditions. Except in silent conditions, they all present bright appearances. Without ultrasound, the surface appears matt with the presence of corrosion products (in light gray) systematically removed during sonication. Ripples are present when ultrasound is applied and show a concentric pattern if frequency sweep is on. A more damaged area is visible (a-c), corresponding to the focal zone, and associated with a disorganized area, resulting from the convective flow induced by the small angle to the vertical axis of the sample. It can be seen that dissolution is less efficient compared to Fig. 3, where a hole was observed for ΔF < 0. This is in agreement with the decrease in total dissolution rates. Besides, break-away craters can be observed on the magnesium alloy surface, which were not seen for pure Mg. They arise from solid matter removal, which indicates a change in the erosion mechanism.

Corresponding SEM pictures are presented in Fig. 14. They confirm that, whatever the conditions, sonication removes corrosion products. Crater depth was measured to be 400 – 700 μm. While the overall appearance is similar to that observed in the case of pure Mg, here the presence of concentric ripple patterns, as well as crater depth, are attenuated. Looking closer, a profilometry surface analysis (Fig. 15a & 15b) at the ripple organization on the right side of the ΔF < 0 sample, where it is more pronounced, reveals a succession of regularly arranged peaks and valleys.

The 2D and 3D surfometry pictures show large valleys around 100 μm wide separated by peaks. This observation is similar to that made on pure Mg (Fig. 6) but with less clearly defined ridge lines and a rougher surface.

Once again, a profile was extracted along the radial axis (red line in Fig. 15a) and is plotted in Fig. 16. This profile is far less regular than the one observed on pure Mg, with the presence of many smaller peaks, making peak-to-peak distance more difficult to measure. It was evaluated here to about 200 μm. The amplitude of the oscillations was quantified with a mean height of profile elements Rc of 28 μm, i.e. quite smaller compared to pure Mg (37 μm) as shown in Fig. 7. Besides, while slopes were relatively smooth for pure Mg, with a very simple pattern, uneven profiles with numerous sub-peaks and valleys are observed for the alloy. This irregular pattern makes measurement of micro-roughness non-meaningful, even if an average value at 0.19 μm can be proposed with great care.

The irregular pattern of the peaks slopes makes measurements of the micro-roughness non-uniform. Indeed, random distribution of the grain boundaries on the slopes introduces a large variability. These determinations were repeated for all ultrasonic conditions in the zones where ripples are well organized and are summarized in Table 2. The mean height of profile elements Rc only slightly varies with the sweeping conditions and remains in the same range of magnitude as for pure Mg. However, as the oscillations are not as well delimited, this results in a larger uncertainty in determination of surface oscillation wavelength. Although the latter certainly varies in the intended direction (higher values for ΔF < 0 and ΔF = 0 compared to ΔF > 0), a drift appears in relation to the theoretical wavelengths.

The surface was examined with SEM microscopy (Fig. 17). Contrary to pure Mg, a strong dependence on ultrasonic conditions was observed. While grain boundaries are more attacked than the grains in all cases, the attack is more pronounced in the case of ΔF < 0 (i.e. when the highest mass loss is obtained), where all grain boundaries are cleared. The presence of residual impurities on the surface for fixed frequency and silent conditions is consistent with the lower mass loss rates (Fig. 12).

It can be seen in Fig. 17 that ultrasound effects are especially visible for negative frequency sweep i.e. when cavitation is favoured. On the contrary, when acoustic streaming becomes the major phenomenon, the effects on grains boundaries are drastically reduced, with quite no observable effects. This is why the next observations focused on negative

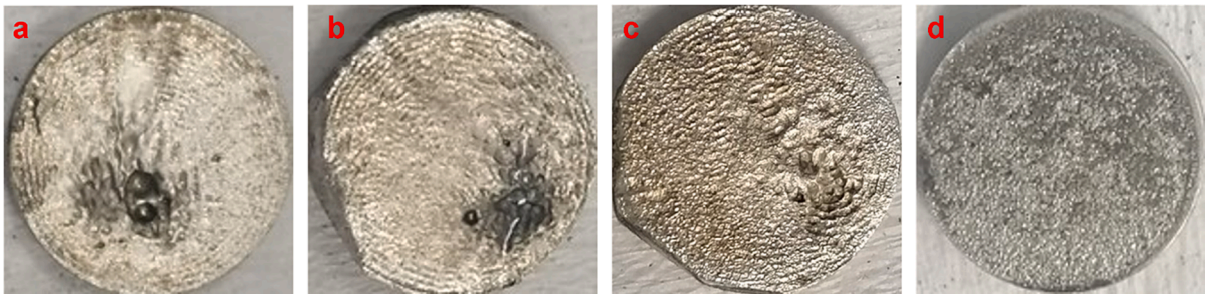

Fig. 13. Photographs of magnesium alloy discs after 20 min of irradiation in 0.1 M oxalic acid under a) negative frequency sweep (3.6–3.44 MHz 2 ms). b) positive frequency sweep (3.6–3.76 MHz 2 ms). c) fixed frequency (3.6 MHz) d) without ultrasound.

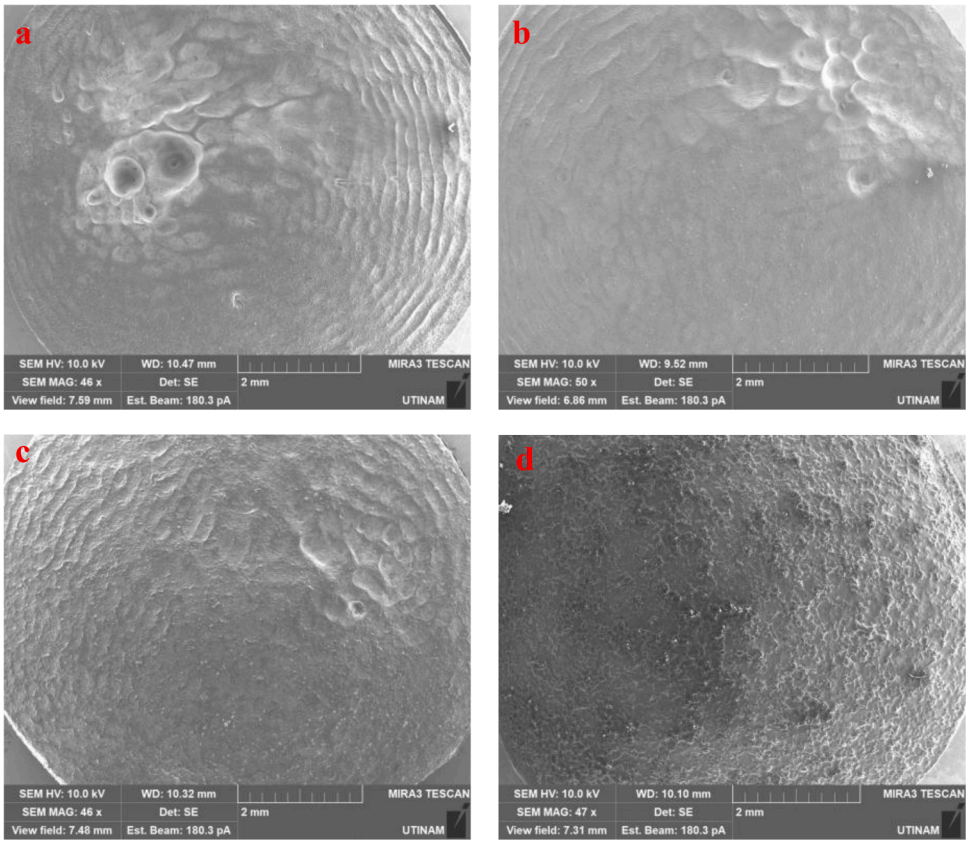

Fig. 14. SEM images of magnesium alloy surfaces after 20 min of irradiation in 0.1 M oxalic acid under. a) $\Delta F < 0$ 3.6–3.44 MHz (2 ms). b) $\Delta F > 0$ 3.6–3.76 MHz (2 ms). c) $\Delta F = 0$. d) without US.

frequency sweep in Fig. 18. Looking closer at the surface (magnification x30000) and using EDS analysis on grains and grain boundaries (Fig. 18), it can be noted that, in oxalic acid dissolution in silent conditions, the surface is rough, which can be attributed to the presence of oxide-based corrosion products (17 % O) [24]. Oxygen content is lower in the depth of grain boundaries, but the latter are not cleared over their entire length. When US is applied under the most efficient conditions ($\Delta F < 0$), oxygen content decreases on the top of the grains, reducing the difference with the grain boundary composition. In all conditions and locations, there is no significant evolution of Mg and alloying element ratios. For comparison, Fig. 18 c. presents the surface obtained after mechanical polishing to ¼ μm and HCl leaching. This treatment leads to an even cleaner surface of the grains, as shown by the lower O content, but with less effect on the grain boundaries, which retained the same chemical composition and are not cleared over their full length. This cleaner surface, with a less efficient protective oxide barrier, is more prone to dissolution

4. Conclusion

Use of focused US and of wobbling makes it possible to highlight the respective contributions of cavitation and acoustic streaming in the dissolution of pure Mg and AZ31 Mg alloy. Dissolution of pure magnesium is very sensitive to US focussing and to wobbling. Under negative sweeping, which leads to an increase in cavitation activity and a decrease in local agitation, very large dissolution rates can be reached at the focal point, up to 150 μm/min. As predicted in former work with SL and SCL measurements, use of a positive sweep induces the reverse effects, with an intense acoustic streaming and a low cavitation activity, and leads to lower dissolution rates. In both cases, surface oxides are removed much faster than in the absence of ultrasound, indicating that the combination of acoustic streaming and mild acidic conditions is sufficient to remove them. Macro- and micro-roughnesses are generated by sonication and are oriented according to the direction of propagation of the US waves. In the particular case of HIFU, micro-roughnesses are

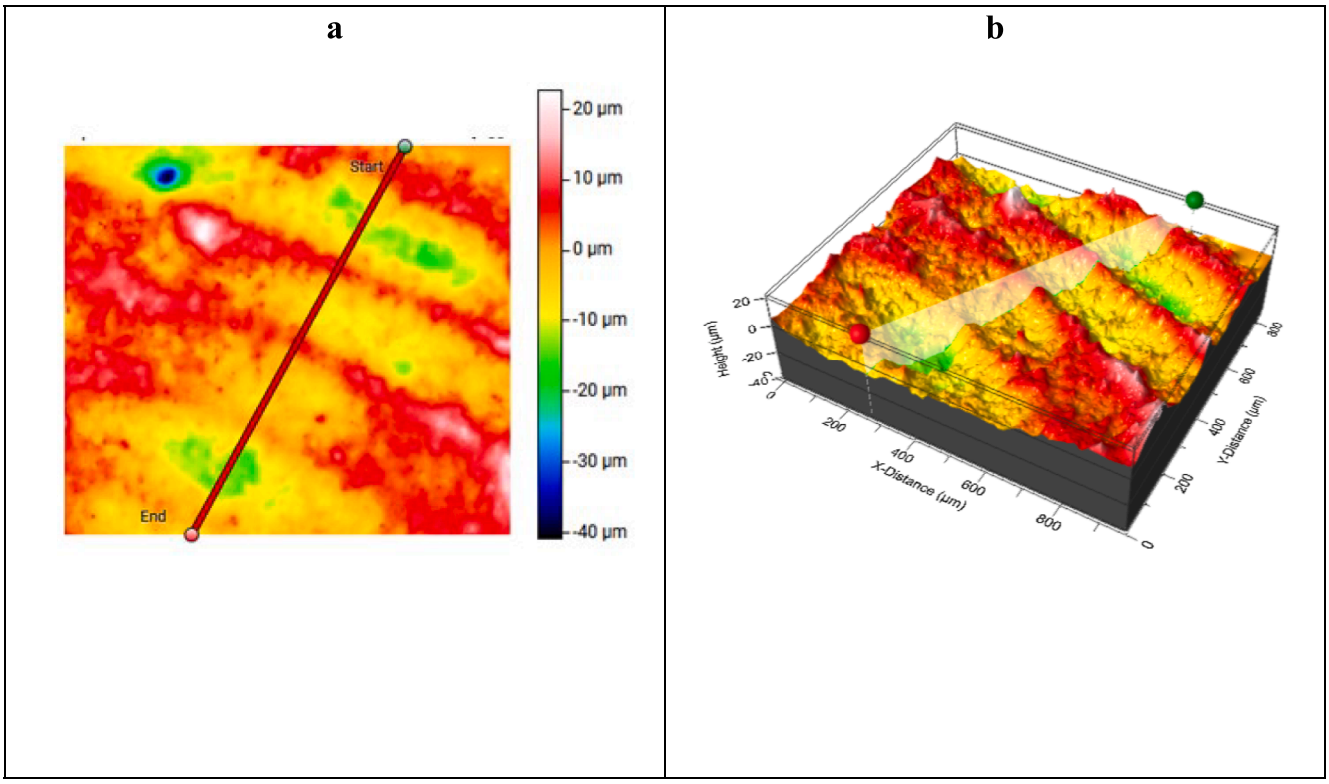

Fig. 15. Magnesium alloy surface profile after 20 min of irradiation in 0.1 M oxalic acid under negative sweeping 3.6–3.44 MHz (2 ms) with an interferometer: a) 2D profile, b) 3D profile.

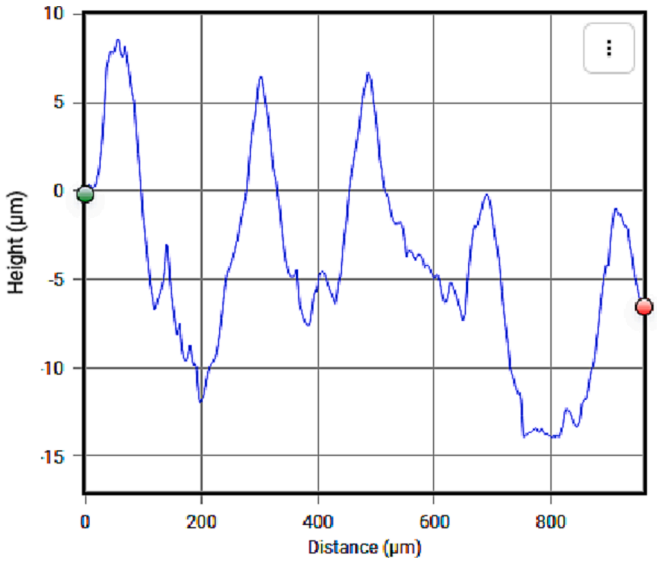

Fig. 16. Magnesium alloy surface profile after 20 min of irradiation in 0.1 M oxalic acid under negative sweeping 3.6–3.44 MHz (2 ms) with an interferometer.

barely modified by ultrasound. We noted at the contrary that riddles, which can be linked to macro-roughness, develop in a centrifugal manner, starting at the center on the focal area. The macro-roughness pattern corresponds to average wavelengths of the wobbling range, for all three cases ($\Delta F < 0$, $\Delta F > 0$, $\Delta F = 0$).

Observations are more complex in the case of the Mg alloy, where dissolution rates are independent from the sweeping mode. The dissolution mechanism is different from the pure Mg case: less sensitive to cavitation erosion but more sensitive to acoustic streaming induced

Table 2
Oscillation period and half acoustic wavelength for pure Mg under $\Delta F < 0$, $\Delta F > 0$ and $\Delta F = 0$.

Conditions	Irradiation conditions	Mean frequency, MHz	Theoretical $\lambda/2$, µm	Surface oscillation wavelength, µm	R_c, µm
$\Delta F < 0$	3.6–3.44 MHz 2 ms	3.52	213	200	28
$\Delta F > 0$	3.6–3.76 MHz 2 ms	3.68	204	197	33
$\Delta F = 0$	3.6 MHz	3.6	208	216	26

dissolution. Preferential attack of the grain boundaries is observed, even if grain surfaces are also attacked. This difference between more ductile pure Mg and the harder and more cavitation-resistant Mg alloy indicates the limits of the combination of focused US in wobbling mode. It is to be noted that, even if joint grain dissolution cannot be controlled, this technique is extremely efficient in revealing the microstructure.

CRediT authorship contribution statement

Noura Sleiman: Investigation, Writing – original draft. **Rachel Pflieger:** Conceptualization, Methodology, Writing – review & editing. **Loïc Hallez:** Conceptualization, Investigation, Methodology, Writing – review & editing. **Sergey I. Nikitenko:** . **Jean-Yves Hihn:** Conceptualization, Investigation, Supervision, Writing – review & editing.

Declaration of competing interest

The authors declare that they have no known competing financial interests or personal relationships that could have appeared to influence the work reported in this paper.

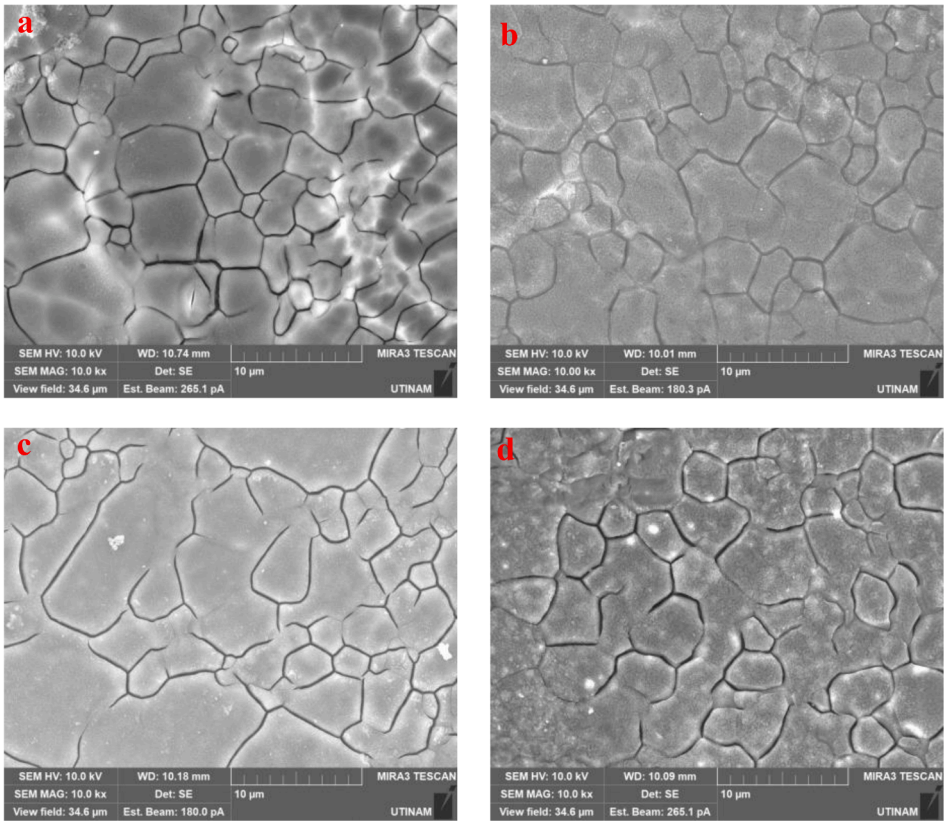

Fig. 17. SEM image of magnesium alloy surface after 20 min of irradiation in 0.1 M oxalic acid under. a) $\Delta F < 0$ 3.6–3.44 MHz (2 ms). b) $\Delta F > 0$ 3.6–3.76 MHz (2 ms). c) $\Delta F = 0$. d) without US.

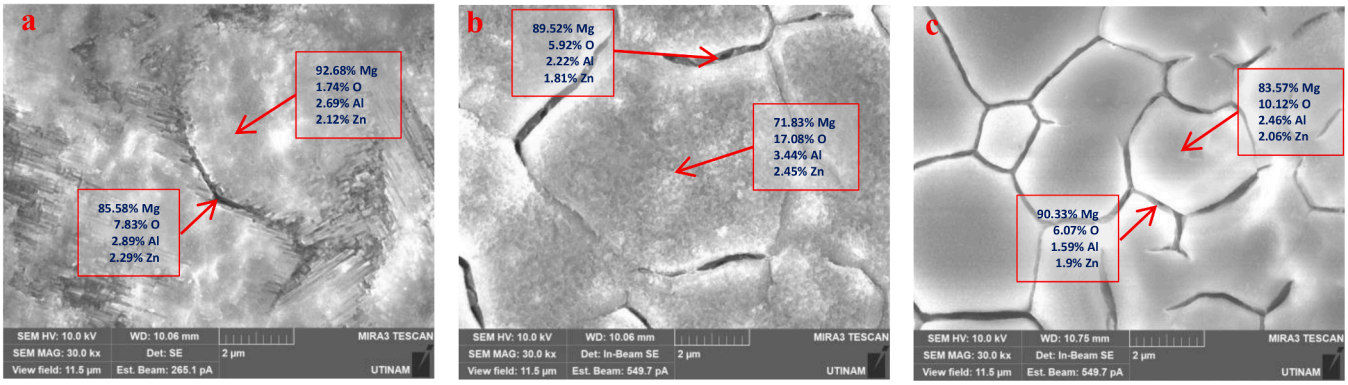

Fig. 18. SEM images showing grain boundaries with weight percentage for each element at the grain and grain boundaries. a) sample without US with grain boundaries revealed by 2 % HCl 20 s (polished up to ¼ µm). b) sample immersed for 20 min in oxalic acid without US. c) sample irradiated for 20 min with negative sweeping frequency 3.6–3.44 MHz (2 ms) in oxalic acid.

Data availability

No data was used for the research described in the article.

Acknowledgements

The authors would like to express their acknowledgements to the IRT M2P Metz for its financial support (RESEM VOBUSURF and SPEC-TRUSEB projects). The authors would like to heartily thank the QUALIO laboratory and especially Ms. Sylvaine LINGET for her assistance (ICP measurements). The authors also thank the UTINAM chemistry platform PCU and especially Mr. Nicolas ROUGE for his precious help (SEM/EDS analysis), Ms. Sandrine MONNEY for her assistance (AFM measurements), and Ms. Severine LALLEMAND for her precious advice and time in sample preparation.

References

[1] M.L. Doche, J.Y. Hihn, A. Mandroyan, R. Viennet, F. Touyeras, Influence of ultrasound power and frequency upon corrosion kinetics of zinc in saline media, Ultrason. Sonochem. 10 (6) (2003) 357–362.
[2] S. Vieira Pereira, F. Belotti Colombo, L. Alexandre Pedro de Freitas, Ultrasound influence on the solubility of solid dispersions prepared for a poorly soluble drug, Ultrason. Sonochem. 29 (2016) 461–469.
[3] T. Tekin, D. Tekin, M. Bayramoglu, Effect of ultrasound on the dissolution kinetics of phosphate rock in HNO3, Ultrason. Sonochem. 8 (4) (2001) 373–377.
[4] J.R.G. Sander, B.W. Zeiger, K.S. Suslick, Sonocrystallization and sonofragmentation, Ultrason. Sonochem. 21 (6) (2014) 1908–1915.

[5] T.I. Trofimov, M.D. Samsonov, S.C. Lee, N.G. Smart, C.M. Wai, Ultrasound enhancement of dissolution kinetics of uranium oxides in supercritical carbon dioxide, J. Chem. Technol. Biotechnol. 76 (12) (2001) 1223–1226.
[6] H. Grénman, E. Murzina, M. Rönnholm, K. Eränen, J.-P. Mikkola, M. Lahtinen, T. Salmi, D. Yu. Murzin, Enhancement of solid dissolution by ultrasound, Chem. Eng. Process.: Process Intensification 46 (9) (2007) 862–869.
[7] I. Tzanakis, W.W. Xu, D.G. Eskin, P.D. Lee, N. Kotsovinos "In situ observation and analysis of ultrasonic capillary effect in molten aluminium" Ultrasonics Sonochemistry, Volume 27, 2015, p. 72-80.
[8] S. Cabanas-Polo, K.S. Suslick, A.J. Sanchez-Herencia, Effect of reaction conditions on size and morphology of ultrasonically prepared Ni(OH)2 powders, Ultrason. Sonochem. 18 (4) (2011) 901–906.
[9] K.S. Suslick, D.J. Casadonte, S.J. Doktycz, The effects of ultrasound on nickel and copper powders, Solid State Ion. 32 (3) (1989) 444–452.
[10] D. Worsley, A. Mills, The effect of power ultrasound on the oxidative dissolution of RuO2.xH2O by bromate ions, Ultrasonics 30 (5) (1992) 333–341.
[11] V. Ligier, J.Y. Hihn, M. Wéry, M. Tachez, The effects of 20 kHz and 500 kHz ultrasound on the corrosion of zinc precoated steels in [cl-] [SO4 2-] [HCO3-] [H2O2] electrolytes, J. Appl. Electrochem. 31 (2) (2001) 213–222.
[12] M.L. Doche, J.Y. Hihn, F. Touyeras, J.P. Lorimer, T.J. Mason, M. Plattes, Electrochemical behaviour of zinc in 20 kHz sonicated NaOH electrolytes, Ultrason. Sonochem. 8 (3) (2001) 291–298.
[13] J. Hoffmann, C. Thiebaut, M. Riondet, P. Lhuissier, S. Gaudion, M. Fivel, Comparison of acoustic and hydrodynamic cavitation: Material point of view, Physics of Fluids 35, Issue 1, 2023, article n°017112.
[14] R. Ji, M. Virot, R. Pflieger, R. Podor, X. Le Goff, S.I. Nikitenko, Controlled "golf ball shape" structuring of mg surface under acoustic cavitation, Ultrason. Sonochem. 40 (2018) 30–40.
[15] P. Kanthale, M. Ashokkumar, F. Grieser, Sonoluminescence, sonochemistry (H2O2 yield) and bubble dynamics: frequency and power effects, Ultrason. Sonochem. 15 (2) (2008) 143–150.
[16] R.A. Fowler, S.L. Fossheim, J.L. Mestas, J. Ngo, E. Canet-Soulas, C. Lafon, Non-invasive magnetic resonance imaging follow-up of sono-sensitive liposome tumor delivery and controlled release after high-intensity focused ultrasound, Ultrasound in Medecin and Biology 39 (12) (2013) 2342–2350.
[17] P. Gelat, G. Ter Haar, N. Saffari, The optimization of acoustic fields for ablative therapies of tumours in the upper abdomen, Physics in Medecine and Biology 57, Issue 24, 2012.
[18] L. Hallez, F. Touyeras, J.Y. Hihn, Y. Bailly, Interactions HIFU/POLYMER films, Phys. Procedia 3 (3) (2010) 179–184.
[19] L. Hallez, F. Touyeras, J.Y. Hihn, J. Klima, J.L. Guey, M. Spajer, Y. Bailly, Characterization of HIFU transducers designed for sonochemistry application: cavitation distribution and quantification, Ultrasonics 50 (2) (2010) 310–317.
[20] L. Hallez, F. Touyeras, J.Y. Hihn, Y. Bailly, Characterization of HIFU transducers designed for sonochemistry application: acoustic streaming, Ultrason. Sonochem 29 (2016) 420–427.
[21] H. Chen, X.J. Li, M.X. Wan, S.P. Wang, High-speed observation of cavitation bubble cloud structures in the focal region of a 1.2 MHz high-intensity focused ultrasound transducer, Ultrason. Sonochem. 14 (3) (2007) 291–297.
[22] J. Lee, M. Ashokkumar, S. Kentish, F. Grieser, Determination of the size distribution of sonoluminescence bubbles in a pulsed acoustic field, J. Am. Chem. Soc. 127 (48) (2025) 16810–16811.
[23] L. Hallez, J. Lee, F. Touyeras, A. Nevers, M. Ashokkumar, J.Y. Hihn, Enhancement and quenching of high-intensity focused ultrasound cavitation activity via short frequency sweep gaps, Ultrason. Sonochem. 29 (2016) 194–197.
[24] J. Lee, L. Hallez, F. Touyeras, M. Ashokkumar, J.Y. Hihn, Influence of frequency sweep on sonochemiluminescence and sonoluminescence, Ultrasonics Sonochemistry 64, 2020, article n°105047.
[25] N. Sleiman, L. Hallez, R. Pflieger, S.I. Nikitenko, J.Y. Hihn, Sonoluminescence emission spectra of a 3.6 MHz HIFU in sweeping mode, Ultrasonics Sonochemistry 83, 2022, article n°105939.
[26] J.F. Yan, Nathan N.M. Heckman, L. Velasco, A.M. Hodge, Improve sensitization and corrosion resistance of an Al-Mg alloy by optimization of grain boundaries, Scientific Reports 6, 2016, article n°26870.
[27] G.L. Song, Corrosion electrochemistry of magnesium (Mg) and its alloys, Woodhead Publishing Series Metals Surf. Eng. (2011) 3–65.